Prognostic Significance of Biointegration at the Optic–Cornea Joint in Keratoprosthesis Implantation

Esen Karamursel Akpek, MD,* Anthony J. Aldave, MD,† Guillermo Amescua, MD,‡
Kathryn A. Colby, MD, PhD,§ Maria S. Cortina, MD,¶ Jose de la Cruz, MD,¶
Jean-Marie A. Parel, PhD,‡ and James W. Foster, PhD*

Purpose: The purpose of this study was to characterize the morphological and immunological aspects of biointegration at the optic–cornea joint of a second-generation synthetic corneal device.

Methods: The initial prototype, single-piece optic–skirt configuration, is constructed from compact and flexible perfluoroalkoxy alkane with porous expanded polytetrafluoroethylene (ePTFE) overlying the skirt to allow skirt–cornea biointegration. The second-generation version was modified to add ePTFE around the optic wall to allow optic–cornea biointegration. Initial and amended second-generation devices were implanted into healthy rabbit eyes. Clinical examination, anterior segment optical coherence tomography, light microscopy, and immunofluorescence studies were performed to assess structural integrity and determine molecular signatures indicative of inflammation and tissue remodeling between the 2 prototypes.

Results: Recipient eyes with both device versions showed no epithelial defects or tissue retraction at 3 months postoperatively. Optical coherence tomography images demonstrated no appreciable perioptic space with either prototype. Histopathology of the initial device demonstrated lack of stromal adhesion at the optic–cornea joint with epithelium filling the perioptic space. Second-generation devices demonstrated full sealing of the recipient stroma along the optic stem. Although the routine histopathology did not demonstrate inflammatory cells in the recipient cornea with either device, immunohistochemistry stains demonstrated quiescent phenotype of stromal and epithelial cells only in the second-generation devices.

Conclusions: Biointegration between the synthetic corneal device and recipient tissue at the optic–cornea joint seems to avert inflammation and may help prevent sterile tissue lysis and prolong retention.

Key Words: keratoprosthesis, corneal transplantation, immunohistochemistry

(*Cornea* 2024;00:1–9)

Donor corneal transplantation, also known as keratoplasty, remains the mainstay to restore sight in individuals with vision loss due to loss of corneal transparency. Keratoplasty is a highly successful transplantation procedure with an over 90% graft clarity rate at 2 decades postsurgery as reported previously.[1–3] However, not all patients enjoy favorable outcomes. Graft failure is not uncommon in certain clinical circumstances such as young recipient age, history of coexisting glaucoma or glaucoma surgeries, aphakia, corneal vascularization, iridocorneal adhesion, or ocular surface disease.[4] Unfortunately, both graft survival and visual outcomes worsen with each successive graft.[5] Importantly, prior graft failure is currently the leading preoperative indication for penetrating keratoplasty in North America and Europe.[6–10]

The idea of implanting a transparent synthetic device to aid in the passage of light to the photosensitive retina is not new. In fact, the first keratoprosthesis (KPro) surgery was reported in 1855.[11] For patients who are at high risk of failure with donor keratoplasty, prosthokeratoplasty or artificial corneal transplantation is a viable and often the only option to restore sight. Although several devices are currently available for clinical use, none is free of postoperative complications, with worsening outcomes over longer term follow-up, even with close postoperative monitoring.[12–15]

The 3 main characteristics of an ideal artificial cornea were summarized previously[16]: 1) flexibility to prevent irritation and tissue inflammation, 2) strong bonding and biointegration to the recipient cornea to withstand intraocular pressure and trauma, and 3) complete epithelization. Significant improvements in our understanding of corneal biology and strategies to optimize device biocompatibility have been made in more recent years. Surface modifications to enable

bonding between the rigid devices and recipient cornea with extension of the extracellular matrix and viable cellular elements into the device (biointegration) have been attempted and resulted in some improvement of the outcomes.[17–20] Synthetic devices with flexible skirt configuration to improve biointegration introduced at the turn of the century.[21] were able to lower the risk of postoperative glaucoma but were associated with stromal melting and optic fouling likely due to the inherent issues with the materials used.[22] In addition, advanced bioengineering approaches to form replacement corneas continue. Certain biomolecules such as collagen are being investigated to create corneal substitutes using 3-dimensional bioprinting.[23] Alternatively, decellularized corneas from nonhuman mammalian sources have also shown potential in replicating both corneal composition and fibril architecture.[24]

With the goal of creating a corneal prosthesis with more favorable clinical outcomes, we designed a single-piece, fully synthetic, flexible, sutureable optic–skirt configuration device prototype. Biocompatibility of the materials used for optic and skirt sections, dimensions and anatomical considerations for the device configuration, feasibility of the novel surgical technique, and clinical outcomes of 2 different prototypes have been previously published.[25,26] We herein report the improvements made to the optic–skirt joint to enhance biointegration and their direct impact on clinical outcomes in a healthy rabbit model.

MATERIALS AND METHODS

The study protocols (RB17M34 and RB23M12) were approved by the Johns Hopkins University Animal Care and Use Committee, Baltimore, Maryland. The Association for Research in Vision and Ophthalmology's statement for the Use of Animals in Ophthalmic and Vision Research and tenets of the Declaration of Helsinki regarding the ethical treatment of animal subjects were adhered to throughout the study.

Prosthesis

The research device is a single-piece, flexible, fully synthetic prosthesis made out of transparent and compact perfluoroalkoxy alkane (PFA) (proprietary to W.L. Gore & Associates, Inc., Newark, DE) (Fig. 1) that is resistant to biofouling.[25–27] The skirt, secured with permanent sutures within a lamellar stromal pocket, houses 16 macroapertures for diffusion of fluid and nutrients to the anterior corneal lamella from the aqueous humor, to prevent desiccation. The skirt is overlaid with a porous ingrowth surface using expanded polytetrafluoroethylene (ePTFE) in an effort to improve the integration of the corneal stroma at skirt–cornea joint. The ePTFE layer is bonded in a biologically inert manner to minimize the risk of separation/peeling and tissue irritation postimplantation. The ingrowth surface is rendered hydrophilic with a temperature-resistant polyvinyl alcohol-based coating and becomes translucent when wetted. Upon implantation, the optic lies within a central, full-thickness
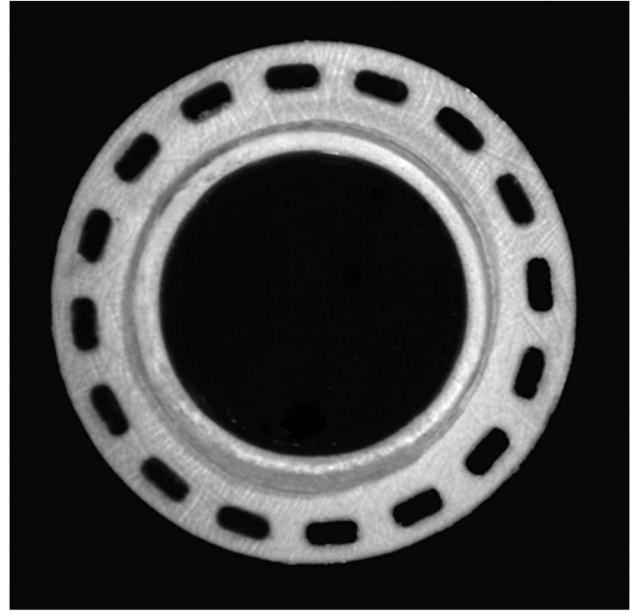

FIGURE 1. External photograph of the novel, single-piece, optic–skirt configuration, fully synthetic artificial corneal device. The skirt houses 16 macroapertures to allow diffusion of fluid and nutrients to the anterior lamella. The optic is clear, and the skirt (white) is laid with a porous ingrowth surface made out of expanded polytetrafluoroethylene.

corneal trephination site, extending between the ocular surface anteriorly and anterior chamber posteriorly.[25,26]

The device optic diameter measures 4.75 mm anteriorly and 4.25 mm posteriorly and has a central thickness of 0.9 mm. The skirt has an outer diameter of 6.9 mm, and the thickness at the outer edge is 0.2 mm.

The optic wall was amended during the making of the second-generation devices (Figs. 2, A, B). The porous ePTFE ingrowth surface was fused onto the optic wall 360 degrees to allow for full biointegration along the entire optic–cornea joint. In addition, a microflange was placed around the anterior perimeter of the optic for protection of the adjacent corneal epithelium from microtrauma with each blink. The device weighs approximately 38 mg, which is less than the weight of an average (8 mm) human corneal button (50 mg) or Boston type I keratoprosthesis (KPro) with an 8.5-mm titanium plate (80 mg), without the donor corneal carrier.

Surgical Technique

Details of the surgical technique with a short video and postoperative care have previously been published.[26] New Zealand white rabbits aged 12 months and older were used for all experiments. The surgery was performed in the right eye of each rabbit using an operating microscope with built-in optical coherence tomography (OCT) (Proveo 8 Ophthalmic Microscope, Leica Microsystems, Wetzlar, Germany). Briefly, an initial partial-thickness trephination at 60% to 70% of the corneal thickness was made using a 4.0-mm disposable, handheld metal trephine (Surgistar, Vista, CA).

FIGURE 2. Optic wall configuration of the initial (A) and second-generation (B) devices. The top section shows the diagram of the devices (all dimensions are in mm, drawn to scale), and the bottom section shows the corresponding actual side view using a microscope (Nikon SMZ1500 stereomicroscope, magnification ×15). The initial device optic stem (A) has a plain wall without an ingrowth surface. The second-generation device optic stem (B) is laid with biocompatible, porous expanded polytetrafluoroethylene in its entire wall to boost tissue adhesion at the optic–cornea joint and avert postoperative perioptic space. A microflange was also placed around the optic perimeter anteriorly to protect adjacent corneal epithelium from microtrauma due to blinking. The skirt in both device constructs is identical and covered with ePTFE to allow tissue adhesion at the skirt–cornea joint. (The full color version of this figure is available at www.corneajrnl.com.)
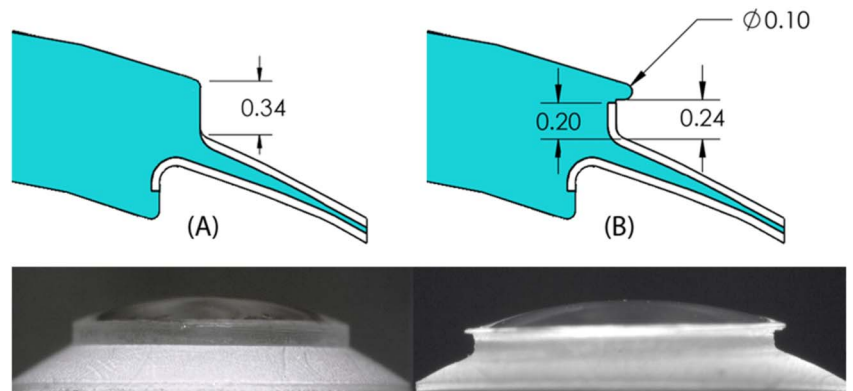
Then, an intrastromal lamellar pocket measuring 8 mm in diameter was created 360 degrees manually around the trephination site, using a disposable 2.2-mm angled, double-bevel spoon blade (Unique Technologies, Mohnton, PA). The anterior chamber was then penetrated through a paracentesis using a 15-degree surgical blade (I-Knife, Alcon, Fort Worth, TX) and filled with an ophthalmic viscoelastic (HEALON, Johnson & Johnson Surgical Vision, Santa Ana, CA). The 4-mm central corneal button was removed full thickness using a pair of curved microscissors (Vannas Capsulotomy Scissors, Ambler Surgical, Exton, PA). The device was then folded and inserted within the intrastromal pocket and sutured in place using 16 interrupted 10-0 nylon sutures (CS160-6, Ethicon, Cornelia, GA) with the knots buried into the host stromal rim. The viscoelastic was removed from the anterior chamber via the paracentesis and replaced with balanced salt solution. The paracentesis was closed using a single 10-0 nylon suture. Nineteen rabbits underwent surgery using the initial device,[25] and 16 rabbits received the second-generation device.[26]

Examinations and Data Collection

Clinical examinations were performed under general anesthesia using an operating microscope. Fluorescein drops and cobalt blue light were used to assess epithelial defects, guttering alongside the optic, and thinning or retraction of the anterior lamella overlying the skirt. Device–cornea complex was imaged through the operating microscope with built-in OCT to assess the anterior and posterior corneal lamellae and apposition of the device within the recipient stroma.

Control Eyes

The unoperated left eyes of all rabbits that received surgery were enucleated at the time of euthanasia to serve as negative controls. For positive control, an alkali-burn model was elected. After deep anesthesia was induced, alkali burn was performed in OU of a syngeneic rabbit by placing a 7.00-mm diameter disc of #40 Whatman filter paper (Fisher Scientific, Hampton, NH) saturated with 4M sodium hydroxide on the central cornea for 1 minute. The cornea was irrigated copiously with 0.9% saline. The epithelium was then debrided full thickness with a sterile cotton-tipped applicator to create a defect measuring 7 mm in diameter. The rabbit was treated with a subcutaneous narcotic analgesic applied every 72 hours for pain control and erythromycin ointment applied 6 times daily for ocular comfort and infection prophylaxis in the operated eye. The rabbit was examined daily using penlight and euthanized after 7 days postburn. OU were harvested. A single failed initial design device with clinically apparent tissue thinning and retraction around the optic perimeter (Fig. 3) was also studied to further validate the relevance of the reagents used to assess the inflammatory mediators present in the recipient corneal tissue.

Histopathology and Immunohistochemistry

For histopathology, the eyes were enucleated after having been marked for orientation, fixed in Bouin's solution for 48 hours, and preserved in 10% neutral buffered formalin until trimming. The implant in situ was trisected on the perpendicular plane and embedded in paraffin and serially sectioned at 200 μm intervals through the entire block. Two 5-μm thick slides were made at each section: 1 stained with hematoxylin and eosin (H&E) and 1 stained with Masson's trichrome. In addition, a cross-section of the lens and optic nerve from each globe was embedded in paraffin, and sections were stained with H&E and Masson's trichrome.

For immunofluorescence studies, the enucleated eyes were fixed in Davidson's fixative overnight and then stored in neutral buffered formalin until processed. Slides were deparaffinized with three 5-minute washes in Histo-Clear (VWR, 64110-04, Radnor, PA) and then rehydrated in

FIGURE 3. Clinical appearance of the rabbit eye under cobalt blue light showing fluorescein dye take-up indicating tissue retraction and thinning highlighted with a red arrow (left image) and corresponding area in anterior segment OCT image confirming the findings of tissue separation from the optic (right image). (The full color version of this figure is available at www. corneajrnl.com.)
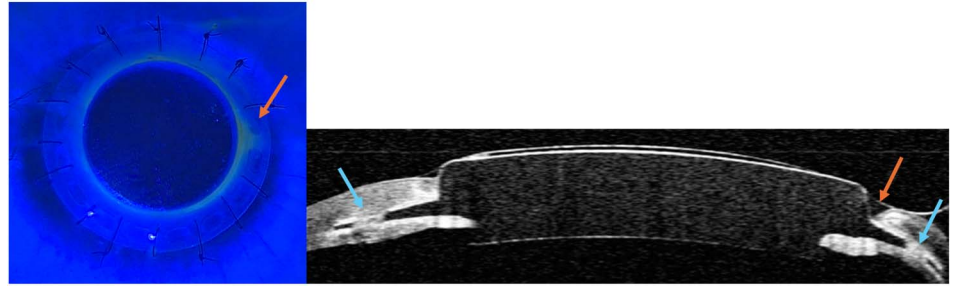
100% (twice), 95%, 70%, 50%, and 30% ethyl alcohol. Slides were washed in deionized water and then unmasked by incubating in TRIS-EDTA buffer at 98°C for 30 minutes. Slides were equilibrated in phosphate buffered saline (PBS) and then permeabilized in 0.2% Triton X100 for 15 minutes. Slides were blocked in blocking buffer 3% bovine serum albumin and 2% normal goat serum in PBS for 1 hour. Selected primary antibodies (Table 1) were then incubated overnight at 4°C and optimized concentrations in blocking buffer.

Slides were washed 3 times, 15 minutes each in PBS, and then incubated with Alexa Fluor 647 conjugated secondary antibodies (Anti-host, Invitrogen) for 1 hour at room temperature. Nuclei were then counterstained with DAPI for 5 minutes, followed by 3 washes in PBS, 15 minutes each and mounted (ProLong Gold Antifade). Images were obtained on an Axio Imager A2 (Carl Zeiss Meditec, Jena, Germany) using AxioVision software.

RESULTS

Clinical Findings and Imaging

All surgeries were completed without damage to lens or iris or other surgical complications, and the results were previously published.[25,26] Clinical findings of the eyes with both earlier and second-generation devices (Fig. 4) were identical and showed no signs of epithelial defects, tissue thinning, or retraction at 3 months postoperative follow-up.

OCT images (Fig. 5) also showed comparable findings between the 2 device constructs with tight apposition of the recipient anterior corneal lamella and optic wall.

TABLE 1. List of Selected Primary Antibodies Used During the Immunofluorescence Evaluations of Tissue Samples

Target	Supplier	Catalog Number	Host	Concentration
α-Smooth muscle actin	ThermoFisher	MA1-06110	Mouse	1:200
Matrix metalloproteinase-9	ThermoFisher	MA5-15886	Mouse	1:500
Proliferating cell nuclear antigen	ThermoFisher	133900	Mouse	1:500
Vimentin	Cell Signaling	5741S	Rabbit	1:200

Neither clinical appearance nor AS-OCT images showed findings that could have prompted concern regarding impending complications such as sterile keratolysis with either device.

Histopathologic examination of the sectioned tissues (Fig. 6) demonstrated retraction of the corneal stroma from the optical wall and epithelium filling the perioptic space in the earlier device version (A). The second-generation device with the ePTFE ingrowth surface laid around the optical stem 360 degrees showed full adherence of the stroma without epithelial undercutting (B).

Molecular Characterization of Positive and Negative Control Eyes at Optic–Cornea Joint

We investigated the expression patterns of key proteins we posited as having a role in implant success. Matrix metalloproteinase (MMP-9), a major catabolic enzyme, was noted to be sequestered in the epithelium of the unoperated control corneas (Fig. 7). In the alkali burn corneas, there was an increase in MMP-9 expression in the stromal keratocytes, particularly those that were migrating into the affected area. Similarly, in the eye implanted with the initial design device and with clinically evident tissue thinning and retraction, there was widespread positivity in the epithelium as well as stromal cells with heightened positivity immediately adjacent to the optic–cornea joint. There were also areas of epithelial downgrowth along the optic wall with robustly positive cells in the apical surface surrounding the anterior portion of the optic. Epithelial hyperplasia and downgrowth are likely a result of stromal retraction from the optic–cornea joint and a major contributing factor to implant failure due to lack of adhesion of the anterior corneal lamella to the optic stem. Proliferating cell nuclear antigen (PCNA) was present in the epithelium of all eyes, with positive staining of the stroma evident in the migratory cells adjacent to the alkali burn corneas. In the samples from the initial device design with stromal melt and retraction, widespread PCNA activity was also observed in the basal cells of the hyperplastic area as well as surrounding the implant and where the endothelial layer should be. This is suggestive of both epithelial downgrowth and activation of all cell types in the recipient cornea indicating a functional degradation state. Vimentin was only weakly expressed in the basal stromal fibroblasts in the naïve cornea. In the alkali burned corneas, vimentin
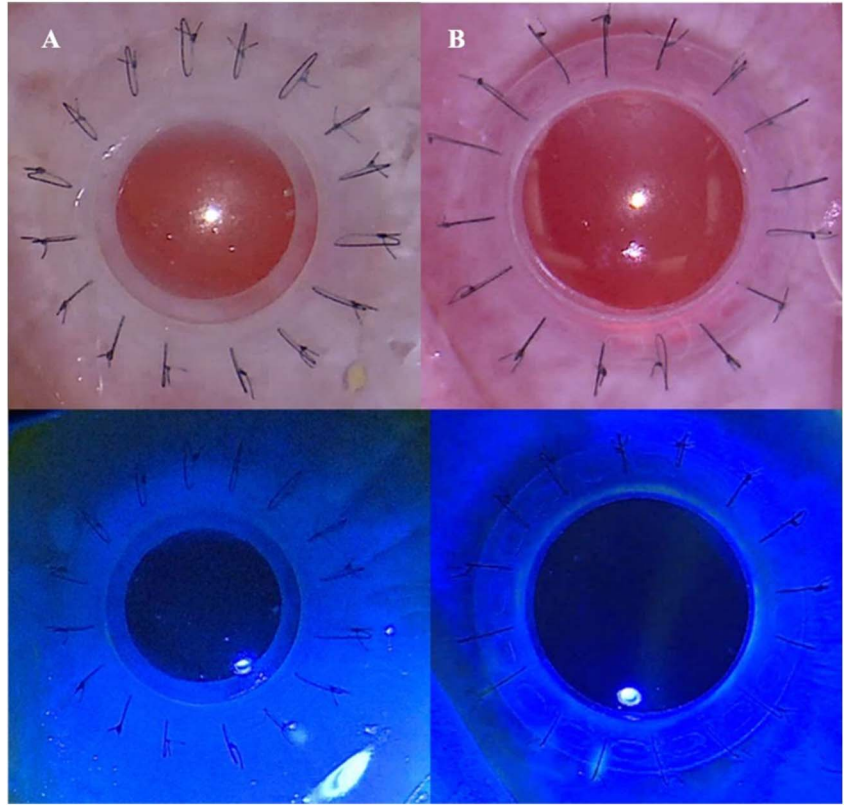
FIGURE 4. Clinical images of the earlier (A) and second-generation (B) devices in situ in rabbit eyes 3 months postoperatively. The device has a semitransparent skirt which is anchored within the corneal stromal pocket with 16 interrupted sutures. Red reflex is evident through the transparent optic cylinder. Fluorescein staining and cobalt blue light examination (bottom pictures) also demonstrated identical findings with no epithelial defect, stromal thinning, neovascularization, or retraction of the recipient cornea at the optic–cornea joint in either prototype. (The full color version of this figure is available at www.corneajrnl.com.)

was present in the apical stromal cells and some of the epithelial cells. In the eye with the initial design device with tissue retraction, there was widespread activation of vimentin across all cell types, though most robustly in the cells that surround the optic stem. Finally, alpha smooth muscle actin (α-SMA) expression was not detected in the naïve cornea but was robustly visualized in the iris. In the alkali burned corneas, there was expression in all layers of the cornea, including at the leading edge of the migrating epithelium around the clinically ulcerated section of the cornea. In the eye with the initial device design with apparent retraction and tissue thinning, this staining pattern was repeated with extensive activation in all cell types,

particularly in the retracting edge of the recipient anterior stroma and epithelium.

## Molecular Characterization of Study Eyes at Optic–Cornea Joint

Molecular analysis of the corneal epithelial and stromal cells interacting with the second-generation device at the device–cornea joint revealed a quiescent phenotype (Fig. 8). PCNA expression, associated with proliferative cells, was observed in the epithelial layer only. The myofibroblast marker α-SMA was only detected in a few basal cells of the epithelium and not in the stroma indicative of a quiescent

FIGURE 5. Anterior segment OCT images of the 2 device constructs at 3 months postoperatively. A, The earlier generation and (B) second-generation prototype (with enhanced optical wall configuration with built-in tissue ingrowth surface). The darker color represents the device, and the lighter color represents the surrounding tissue. The red arrow demonstrates no apparent perioptic space or thinning or retraction of the recipient tissue. (The full color version of this figure is available at www.corneajrnl.com.)
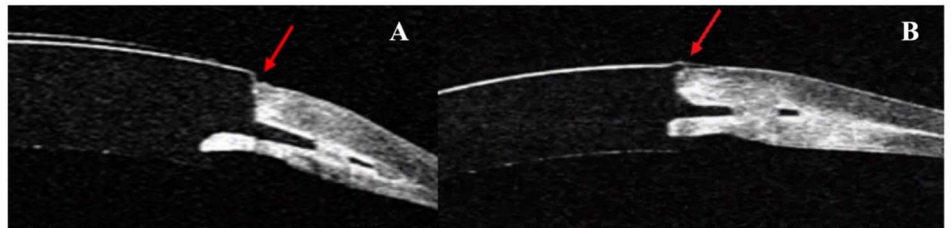
FIGURE 6. Histopathological appearance of the earlier (A) and second-generation (B) devices performed 3 months postoperatively. Although the trichrome stain indicates adhesion of the tissue over the ingrowth surface of the skirt with both prototypes, bonding of the stroma around the optical wall is only evident in the second-generation device (B), with hyperplastic epithelium filling the perioptic space in the earlier generation device (A). The arrow (B) indicates stromal collagen growing through a macroaperture in the skirt. (The full color version of this figure is available at www.corneajrnl.com.)
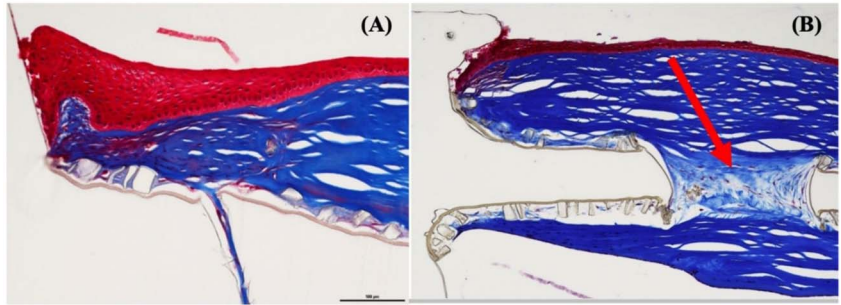
stromal tissue. MMP-9, the major catabolic enzyme in the cornea, was similarly mostly restricted to the epithelial cells, with diffuse staining only seen in stromal cells around the macroapertures in the skirt. This is likely due to migratory stromal keratocytes that are laying the desired de novo matrix. Finally, vimentin was only observed in the cells that are interacting and interspersed with the ingrowth surface. These cells are presumably most actively remodeling the extracellular matrix and thus are more active than the adjacent stromal fibroblasts. On the other hand, the earlier generation device demonstrated similar findings to the positive controls with an increased expression of inflammatory markers, despite the fact that there were no clinical, AS-OCT imaging or histopathological findings suggestive of inflammation.

DISCUSSION

This experimental study proposes the potential prognostic relevance of bioadhesion at the optic–cornea joint in artificial corneal implantation to the retention of the device. Although there were no concerning clinical or OCT imaging findings or any significant inflammation by histopathology in the earlier generation device with biointegration only at the skirt–cornea joint as well as in the second-generation device
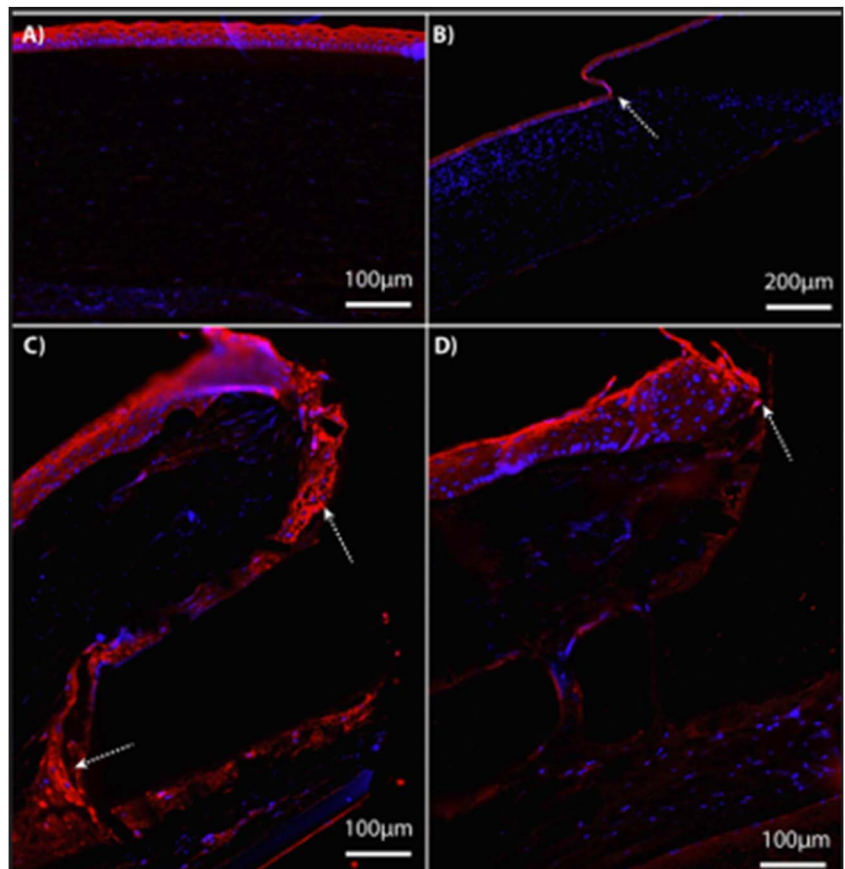

FIGURE 7. Matrix metalloproteinase (MMP-9) expression in the control eyes. The MMP-9 was labeled with red, and nuclei were stained blue (DAPI). The white arrows indicate the areas of staining. All images are oriented from the limbus (left) to the center (right) with the epithelial surface at the top. A, Naïve fellow eye with moderate staining confined only to the epithelium. B, Alkali-burn eye with staining in the anterior stroma devoid of epithelium. C, Earlier generation device eye with clinically apparent tissue retraction and thinning and expression is present in the tissue around the optical stem as well as part of the skirt section. D, Second-generation device eye where there is good adherence of the anterior lamella to the optic stem. MMP-9 staining is confined to the epithelium. (The full color version of this figure is available at www.corneajrnl.com.)
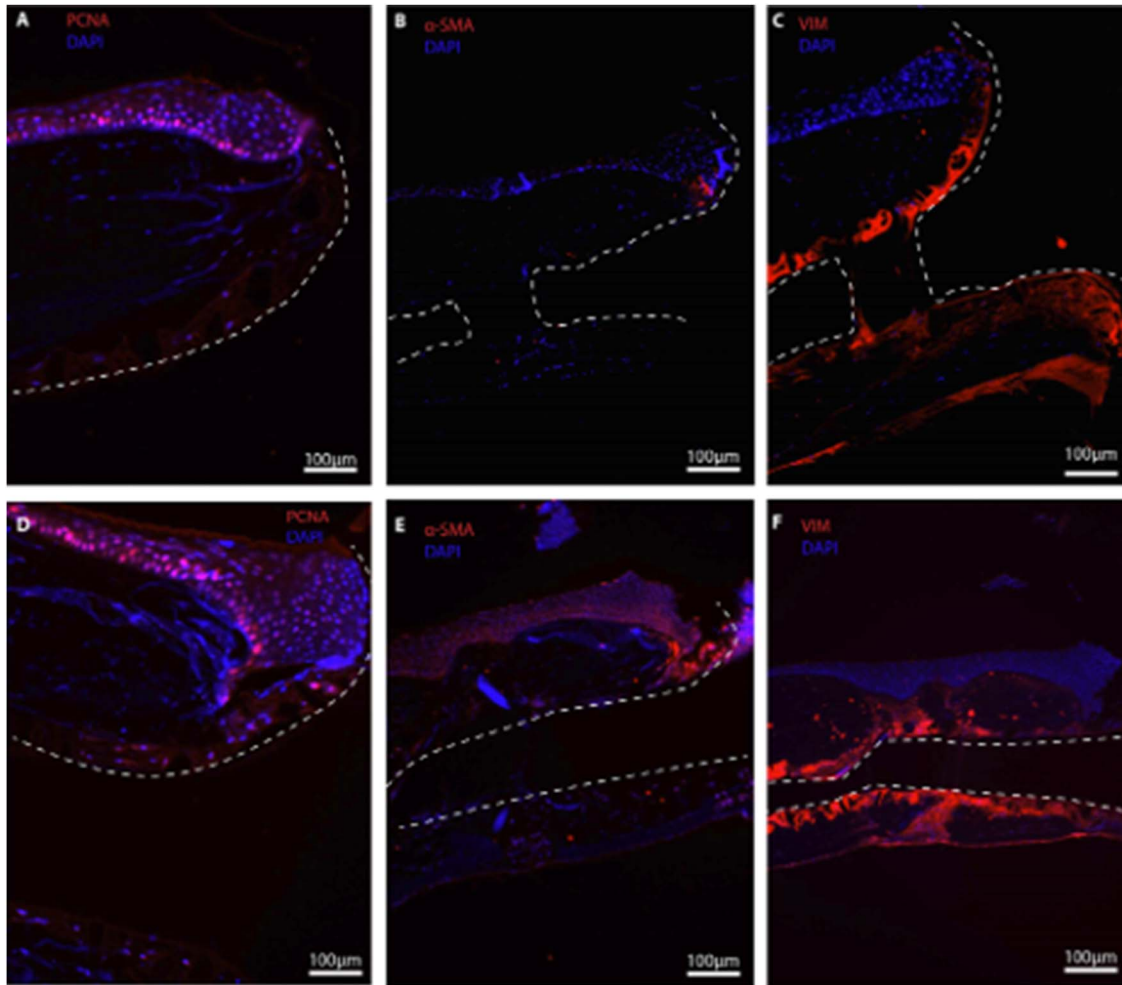
FIGURE 8. Expression of key inflammatory markers assayed at 12 months post-implantation with a second-generation (top) versus at 3 months post-implantation with earlier generation (bottom) device. All images are arranged from the limbus (left) to the center (right), with the dotted white line indicating the solid component of the device with the macroaperture of the skirt in the midsection. In the second-generation device recipient rabbit eye, PCNA expression was restricted to the epithelial cells at the apical surface (A). Expression of alpha smooth muscle antigen (α-SMA) is observed only at the basal cells of the epithelium at the device–cornea interface (B). Vimentin (VIM) expression is only detectable in the stromal cells that are interacting with the ingrowth surface on the top of the skirt (C). In the initial generation device recipient rabbit eye, there is obvious filling of the perioptic space with corneal epithelium with a high expression of PCNA (D) and α-SMA (E) and some tissue detachment at some sections and significant stromal keratocyte expression of VIM (F). (The full color version of this figure is available at www.corneajrnl.com.)

with integration at the optic–cornea and skirt–cornea joints, immunohistochemistry demonstrated quiescent recipient corneal tissue only in the second-generation prototype devices. The second-generation prototype device has an interconnecting porous ePTFE ingrowth surface laid around the optical stem, in addition to the anterior and posterior surfaces of the skirt, which allowed full device–cornea bonding. This device represents a significant step forward toward an ideal artificial cornea, whose features were laid out 25 years ago.[16] The flexibility of the device, allowing full compliance with the recipient cornea,[27] is also a major differentiator from the currently available rigid devices and prevents tissue wear around the optic–cornea junction due to inward flexural

oscillation of the device with each blink and constant outward movement due to intraocular pressure.[25,26] In addition, the macroapertures around the skirt provide tight anchors between the anterior and posterior lamellae of the recipient cornea sandwiching the device that will likely improve the device retention.

The mechanism of improvements made to the second-generation device compared with the initial device design (tissue ingrowth surface, ePTFE, for tissue adhesion laid on the optic stem in addition to the skirt) led to decreased epithelial downgrowth due to full bioadhesion of the stroma at the optic–cornea joint. At 12 months postimplantation, the stroma surrounding the second-generation device (both optic

and skirt) showed new collagenous tissue present at the ingrowth surface. Collagenous matrix was also present in the macroapertures in the skirt designed to facilitate mass transfer and biointegration. However, the placement of the sutures may have exacerbated the proinflammatory environment to a degree as evidenced by the nonaligned, hypercellular matrix that was noted immediately surrounding the in-place sutures (10/0 nylon) in some sections.

We embarked on assaying a panel of markers that we had posited would be markers of potential device failure based on our studies using an alkali corneal burn model and the failed initial design device with clinically apparent sterile stromal melt as positive controls. α-SMA is a marker of myofibroblasts.[28] In the cornea, it is associated with kerato-cyte–myofibroblast transformation and extensive tissue re-modeling, haze formation, and contraction.[21] Its expression, especially in the stromal compartment, should be minimized after wound resolution to prevent scarring.[29] MMP-9 is the major catabolic enzyme of the cornea, and its localization and expression are tightly controlled by several pathways includ-ing the TGFβ pathway.[30] The epithelial layer is the reservoir of MMP-9 in the cornea, and when present in the stroma, it is believed to contribute to modeling, scarring, and melt.[31] PCNA is a marker of mitotically active cells.[32] In the cornea, the endothelial and stromal cells are quiescent, in contrast to the epithelial layer. Expression in the stromal or endothelial cells would be indicative of activation. Finally, vimentin is a marker of activated fibroblasts, which is indicative of early fate decisions in response to a wounding response.[33] Persis-tence in the stromal cells is associated with scarring and failure of wound resolution.[34]

Our results highlight the importance of immune stains in detecting the role of corneal epithelial cells and keratocytes in tissue inflammation. The clinical appearance or OCT images failed to signal any difference between the initial device design and second-generation devices. Routine light microscopy also failed to show any influx of inflammatory cells in the recipient tissues with either device. However, immunofluorescence studies did show presence of prolifera-tive, MMP-9–positive cells on the surface of the unremark-able initial generation device similar to failing initial device design with clinically apparent sterile corneal melt or alkali-burn cornea. Indeed, expression of matrix metalloproteinases in tear fluid, in the setting of Boston keratoprosthesis, has been reported previously in small-scale clinical studies.[31,35] As there are already well-established point-of-care testing tools, testing for MMP-9 levels as an early prognostic indicator for device retention, before obvious signs of tissue thinning, lysis, or retraction, warrants further studying. However, the test can only be applied to tear fluid (vs. corneal tissue) and is qualitative only.

Our work is not without limitations. This is a pre-liminary study with only few specimens examined which precludes definitive conclusions or generalization of the findings. In addition, there may be unknown lack of sensitivity for certain biomarkers used in this study, as there are no prior published reports of markers used within the context of this specific device and the materials it is composed of. All examinations and histopathological evaluations were performed without masking, which could be a potential source of bias. Nonetheless, this is a pilot study with excellent positive and negative control specimens.

In conclusion, this novel, flexible, fully synthetic prototype is a significant advancement toward an artificial corneal device that can potentially be an alternative to donor tissues, particularly in areas of the world without access to a high-cost eye banking system where corneal blindness is most prevalent. An epithelization feasibility study using cultured human corneal epithelial cells is currently underway to be able to meet all 3 attributes of an ideal artificial cornea,[15] flexibility, bioadhesion, and epithelization, to achieve the goal of full biointegration.

REFERENCES

1. Price FW, Whitson WE, Marks RG. Graft survival in four common groups of patients undergoing penetrating keratoplasty. *Ophthalmology*. 1991;98:322–328.
2. Pramanik S, Musch DC, Sutphin JE, et al. Extended long-term outcomes of penetrating keratoplasty for keratoconus. *Ophthalmology*. 2006;113:1633–1638.
3. Fukuoka S, Honda N, Ono K, et al. Extended long-term results of penetrating keratoplasty for keratoconus. *Cornea*. 2010;29:528–530.
4. Claesson M, Armitage WJ. Clinical outcome of repeat penetrating keratoplasty. *Cornea*. 2013;32:1026–1030.
5. Aboshiha J, Jones MNA, Hopkinson CL, et al. Differential survival of penetrating and lamellar transplants in management of failed corneal grafts. *JAMA Ophthalmol*. 2018;136:859–865.
6. Gain P, Jullienne R, He Z, et al. Global survey of corneal transplantation and eye banking. *JAMA Ophthalmol*. 2016;134:167–173.
7. EBAA. Statistical report. Available at: https://restoresight.org/members/publications/statistical-report/. Accessed May 29, 2024.
8. Bigan G, Puyraveau M, Saleh M, et al. Corneal transplantation trends in France from 2004 to 2015: a 12-year review. *Eur J Ophthalmol*. 2018;28:535–540.
9. Flockerzi E, Maier P, Böhringer D, et al. Trends in corneal trans-plantation from 2001 to 2016 in Germany: a report of the DOG-section cornea and its keratoplasty registry. *Am J Ophthalmol*. 2018;188:91–98.
10. Chan SWS, Yucel Y, Gupta N. New trends in corneal transplants at the University of Toronto. *Can J Ophthalmol*. 2018;53:580–587.
11. Chirila TV, Hicks CR. The origins of the artificial cornea: Pellier de Quengsy and his contribution to the modern concept of keratoprosthesis. *Gesnerus*. 1999;56:96–106.
12. Robert M-C, Dohlman CH. A review of corneal melting after Boston keratoprosthesis. *Semin Ophthalmol*. 2014;29:349–357.
13. Crawford GJ. 18 - the development and results of an artificial cornea: AlphaCor™. In: Chirila TV, Harkin DG, eds. *Biomaterials and Regenerative Medicine in Ophthalmology*. 2nd ed. Woodhead Publish-ing; 2016:443–462.
14. Avadhanam VS, Liu CSC. A brief review of Boston type-1 and osteo-odonto keratoprostheses. *Br J Ophthalmol*. 2015;99:878–887.
15. Tsou BC, Koseoglu ND, Akpek EK, et al. Ten-Year outcome of Boston type I keratoprosthesis surgery at a tertiary care center. *Cornea*. 2024;43:982–988. doi.
16. Hicks CR, Fitton JH, Chirila TV, et al. Keratoprostheses: advancing toward a true artificial cornea. *Surv Ophthalmol*. 1997;42:175–189.
17. Salvador-Culla B, Jeong KJ, Kolovou PE, et al. Titanium coating of the Boston keratoprosthesis. *Transl Vis Sci Technol*. 2016;5:17.
18. Riau AK, Venkatraman SS, Dohlman CH, et al. Surface modifications of the PMMA optic of a keratoprosthesis to improve biointegration. *Cornea*. 2017;36suppl 1:S15–S25.
19. Riau AK, Mondal D, Yam GHF, et al. Surface modification of PMMA to improve adhesion to corneal substitutes in a synthetic core-skirt keratoprosthesis. *ACS Appl Mater Inter*. 2015;7:21690–21702.
20. Sawatari Y, Marx RE, Perez VL, et al. Biointegration of the osteo-odonto lamina in the modified osteo-odonto keratoprosthesis: engineering of tissue to restore lost vision. *Int J Oral Maxillofac Implants*. 2013;28:e304–e309.

21. Moshirfar M, Moody JJ, Barke MR, et al. The historical development and an overview of contemporary keratoprostheses. *Surv Ophthalmol.* 2022;67:1175–1199.

22. Holland G, Pandit A, Sánchez-Abella L, et al. Artificial cornea: past, current, and future directions. *Front Med (Lausanne).* 2021;8:770780.

23. Gómez-Fernández H, Alhakim-Khalak F, Ruiz-Alonso S, et al. Comprehensive review of the state-of-the-art in corneal 3D bioprinting, including regulatory aspects. *Int J Pharmaceut.* 2024;662:124510.

24. Procházková A, Poláchová M, Dítě J, et al. Chemical, physical, and biological corneal decellularization methods: a review of literature. *J Ophthalmol.* 2024;2024:1191462.

25. Akpek EK, Van Court S, Glass S, et al. Short-term clinical outcomes of a novel corneal prosthetic device in a rabbit model. *Cornea.* 2020;39:706–712.

26. Akpek EK, Aldave AJ, Amescua G, et al. Twelve-month clinical and histopathological performance of a novel synthetic cornea device in rabbit model. *Transl Vis Sci Technol.* 2023;12:9.

27. Li Gavin, Aldave AJ, Amescua G, et al. Design and biocompatibility of a novel, flexible artificial cornea. *Transl Vis Sci Technol.* 2024;13:19.

28. Jester JV, Petroll WM, Cavanagh HD. Corneal stromal wound healing in refractive surgery: the role of myofibroblasts. *Prog Retin Eye Res.* 1999; 18:311–356.

29. Torricelli AAM, Santhanam A, Wu J, et al. The corneal fibrosis response to epithelial-stromal injury. *Exp Eye Res.* 2016;142:110–118.

30. Li DQ, Lokeshwar BL, Solomon A, et al. Regulation of MMP-9 production by human corneal epithelial cells. *Exp Eye Res.* 2001;73: 449–459.

31. Robert MC, Arafat SN, Spurr-Michaud S, et al. Tear matrix metalloproteinases and myeloperoxidase levels in patients with Boston keratoprosthesis type I. *Cornea.* 2016;35:1008–1014.

32. Gan L, Fagerholm P, Ekenbark S. Expression of proliferating cell nuclear antigen in corneas kept in long term culture. *Acta Ophthalmol Scand.* 1998;76:308–313.

33. Wang X, Qu M, Li J, et al. Induction of fibroblast senescence during mouse corneal wound healing. *Invest Ophthalmol Vis Sci.* 2019;60: 3669–3679.

34. SundarRaj N, Rizzo JD, Anderson SC, et al. Expression of vimentin by rabbit corneal epithelial cells during wound repair. *Cell Tissue Res.* 1992; 267:347–356.

35. Arteaga AC, Weiss MC, Perez R, et al. Metalloproteinase-9 in the ocular surface of patients with implanted Boston type 1 keratoprosthesis. *Cornea Open.* 2023;2:e0008.